Proceedings of ASME 2026 45th International Conference on Ocean, Offshore and Arctic Engineering
OMAE 2026
June 07 – June 12, 2026, Tokyo, Japan

OMAE2026-181476

THE STUDY OF POWER TAKE-OFF SYSTEM SIZING FOR WAVE ENERGY CONVERTER ARRAY

Jian Tan*
Section of Offshore Engineering
Department of Hydraulic Engineering
Delft University of Technology
The Netherlands
Email: J.tan-2@tudelft.nl

Xi Chen
Ocean College
Zhejiang University
China
Email: 12234032@zju.edu.cn

Avni Jain
Section of Offshore Engineering
Department of Hydraulic Engineering
Delft University of Technology
The Netherlands
Email: A.Jain-1@tudelft.nl

George Lavidas
Section of Offshore Engineering
Department of Hydraulic Engineering
Delft University of Technology
The Netherlands
Email: G.Lavidas@tudelft.nl

Hongyi Jiang
Ocean College
Zhejiang University
China
Email: hongyi.jiang@outlook.com

Zhen Guo
Ocean College
Zhejiang University
China
Email: nehzoug@163.com

ABSTRACT

As wave energy converters (WECs) progress toward large-scale commercialization, deployment in arrays is required to achieve higher power capacities, where hydrodynamic interactions strongly influence performance. While Power Take-Off (PTO) systems play a key role in both WEC dynamics and cost, PTO sizing has mainly been studied for standalone devices. This work investigates the combined effects of PTO sizing and array configuration on the techno-economic performance of WEC arrays. A reference array of five heaving point absorbers is analyzed using numerical hydrodynamic modeling with Nemoh and a spectral-domain approach incorporating PTO force capping via statistical linearization, alongside a preliminary cost model. Three representative array configurations are examined, and the results show that PTO sizing is strongly configuration-dependent and can significantly improve overall techno-economic performance, assessed through the levelized cost of energy.

1 Introduction

Ocean wave energy has been recognized as a renewable energy resource for decades, yet its large-scale adoption remains limited compared to offshore wind, solar, and tidal energy. A key obstacle is the non-competitive economic performance of wave energy converters (WECs) [1], with their estimated levelized cost of energy (LCOE) significantly exceeding that of other renewable technologies.

Recent studies have emphasized the importance of developing WECs at the array scale to reduce LCOE. Compared to standalone WEC devices, deploying arrays can lower costs associated with infrastructure, installation, and maintenance. Unlike single WEC devices, the power performance of arrays is influenced by hydrodynamic interactions between devices, making optimal array layouts crucial for maximizing total power production. The configuration of WEC arrays has garnered significant research attention in recent years. For instance, [2] employed a genetic algorithm to optimize array layouts by incorporating both power production and economic factors, presenting and comparing sev-

eral configurations. In [3], a simplified WEC model for point absorbers was introduced to investigate hydrodynamic interactions within arrays. The impact of such interactions on different types of WECs was further analyzed in [4]. Meanwhile, [5] proposed an analytical model to estimate the dynamics of large-scale point absorber arrays, involving up to 1000 devices, and found comparable total power production across configurations, though with notable effects on power fluctuations. Additionally, [6] explored the simultaneous optimization of buoy dimensions and array layouts for point absorber arrays, demonstrating that such an approach enhances total power performance.

Proper sizing of power take-off (PTO) systems is critical for improving the techno-economic performance of wave energy converters [7, 8]. As PTO systems represent a substantial portion of capital expenditure (CAPEX), increasing their capacity significantly raises total costs. However, PTO systems are essential for energy conversion, with their capacity directly influencing power generation. Undersized PTO systems limit maximum force or power output, reducing the WEC's energy absorption capability [8–12]. Studies such as [7, 13–15] have shown that proper PTO sizing can lower the levelized cost of energy (LCOE) by 20% to 30% for single-point absorbers.

The objective of this paper is to analyze the influence of PTO sizing on the techno-economic performance of WECs on an array scale. Five heaving point absorbers WECs are considered in the WEC array, and three different array configurations are taken into account. The PTO sizes of WECs are represented by the maximum PTO force. A spectral-domain (SD) model is established to estimate the dynamics of the WECs, and the PTO force saturation is incorporated through statistical linearization. The hydrodynamic interaction between WECs is analyzed by the open-source software boundary element method solver Nemoh which is linear potential flow theory. The techno-economic performance of the WEC array is reflected by the LCOE, which is calculated by a preliminary economic model. The PTO sizing is implemented for each WEC in the array to minimize the LCOE and a realistic sea site is considered as the environmental input. Based on the results, the relation between the WEC location within the array and the PTO sizing of the individual WEC is identified. Then, the optimized PTO sizes in varied WEC arrays are compared, and the impact of WEC array layout on the PTO sizing is analyzed. Furthermore, the techno-economic performance of WEC arrays with PTO sizing is presented, and the contribution of the PTO sizing to the reduction of the LCOE is revealed.

2 WEC array description

2.1 WEC system

The point absorber WEC concept is depicted in Fig. 1. The floating buoy is modelled as a spherical geometry with a radius of 2.5 m and a density equal to half that of water. The WEC's motion is restricted to heave mode. The buoy is connected to the moving component of a bottom-mounted PTO system, which may function as a piston or generator translator, depending on the PTO type.

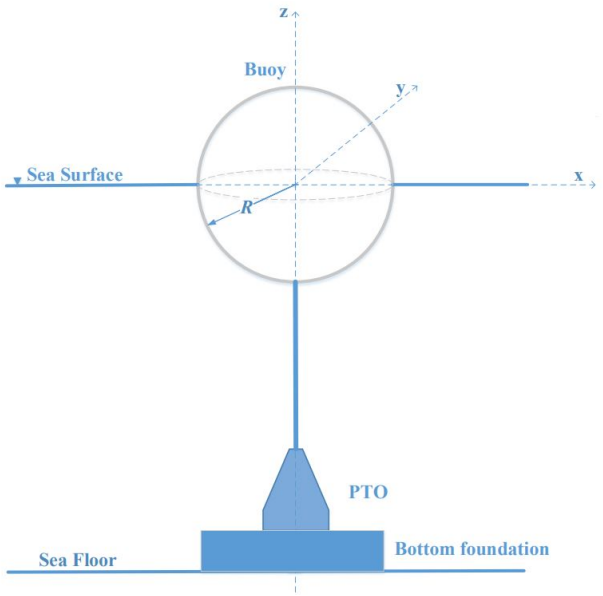

FIGURE 1: SCHEMATIC OF THE SPHERICAL POINT ABSORBER WEC.

2.2 Array configuration

Three different representative array configurations are utilized in this study. This is intended to investigate the impact of array layout on the PTO sizing of the WECs. The geometrical center of each WEC in the arrays is given in Table 1. It should be acknowledged that the considered array layouts are not necessarily optimized for any conditions. They are only used as representatives with clear geometrical variations to reflect the effects of hydrodynamic interactions of WEC arrays. Given the purpose of the work to demonstrate the role of PTO sizing in arrays, it is thought to be a fair implementation. In future work, it would be of interest to incorporate variations in buoy size and inter-device spacing, as these parameters are highly relevant in realistic applications where the available deployment area is constrained. Furthermore, only uni-directional waves are taken into account, in which all waves are assumed to progress along the x-axis from the negative direction to the positive. It is acknowledged that the wave direction is expected to impact the power performance of the WEC array, but it is not investigated in this study given the primary focus of the work.

q factor is widely used in the assessment of the interaction effects of WEC arrays. It is defined as the total power absorption of a WEC array divided by the sum of power absorption

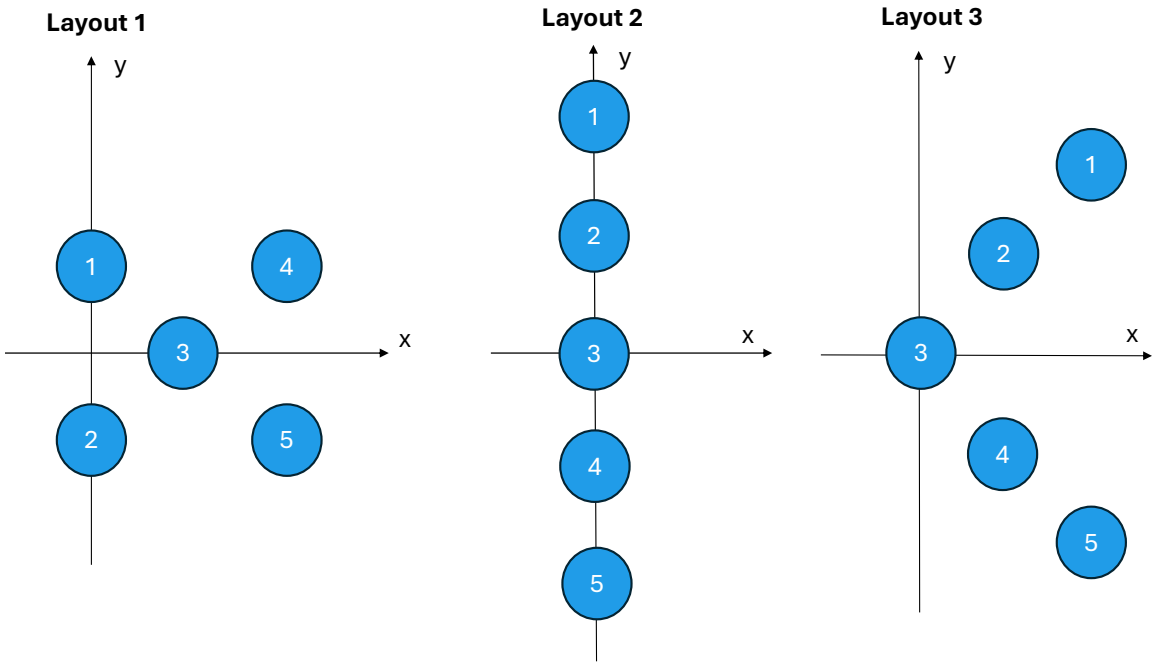

FIGURE 2: SCHEMATIC OF THE THREE CONSIDERED WEC ARRAY LAYOUTS.

TABLE 1: COORDINATES OF WECS IN THE THREE ARRAY CONFIGURATIONS

	Layout 1	Layout 2	Layout 3
WEC 1	(0,7.5)	(0,20)	(14,14)
WEC 2	(0,-7.5)	(0,10)	(7,7)
WEC 3	(7.5,0)	(0,0)	(0,0)
WEC 4	(15,7.5)	(0,-10)	(7,-7)
WEC 5	(15,-7.5)	(0,-20)	(14,-14)

by the same number of isolated WECs. This work is mainly aimed at identifying the PTO sizing effect within a given array configuration, rather than comparing the performance of various array configurations. Hence, a modified q factor is defined here to demonstrate the power performance of each WEC relative to the central WEC, namely WEC 3, in the array:

$$q_{mod,i} = \frac{P_i}{P_3} \tag{1}$$

where $q_{mod,i}$ represents the modified q factor of i_{th} WEC in the array.

3 Methodology

3.1 Numerical modeling

Numerical modelling is adopted in this study to estimate the dynamic responses of the WEC array. As demonstrated in [16], the equation of motion of WEC arrays in the frequency domain is expressed as

$$\begin{aligned} &-\omega^2\left(\mathbf{M}+\mathbf{M_a}(\omega)\right)\vec{\mathbf{Z}}(\omega)+j\omega\left(\mathbf{R_v}+\mathbf{R_r}(\omega)+\mathbf{R_{pto}}\right)\vec{\mathbf{Z}}(\omega) \\ &+\mathbf{K_h}\vec{\mathbf{Z}}(\omega)=\vec{\mathbf{F}_e}(\omega) \end{aligned} \tag{2}$$

where ω is the angular frequency; $\mathbf{M}$ and $\mathbf{M_a}$ represent the mass matrix and added mass matrix of the WEC array; $\mathbf{R_v}$, $\mathbf{R_{pto}}$ and $\mathbf{R_r}$ are the viscous damping matrix, the PTO damping matrix, and the radiation damping matrix of the WEC array; $\mathbf{K_h}$ is the hydrostatic stiffness matrix; $\vec{\mathbf{Z}}$ is the displacement vector of the WEC array; $\vec{\mathbf{F}_e}$ is the excitation force matrix of the WEC array. The sizes of the matrices and the vector are $n \times n$ and $n \times 1$, where n represents the number of WEC devices included in the matrix. To be specific, the mass matrix, added mass matrix, radiation damping matrix, and the hydrostatic stiffness matrix are given as

$$\mathbf{M} = \begin{bmatrix} M_{11} & 0 & \dots & 0 \\ 0 & M_{22} & \dots & 0 \\ \vdots & \vdots & \ddots & \vdots \\ 0 & 0 & \dots & M_{nn} \end{bmatrix} \tag{3}$$

$$\mathbf{M_a}(\omega) = \begin{bmatrix} M_{a_{11}}(\omega) & M_{a_{12}}(\omega) & \dots & M_{a_{1n}}(\omega) \\ M_{a_{21}}(\omega) & M_{a_{22}}(\omega) & \dots & M_{a_{2n}}(\omega) \\ \vdots & \vdots & \ddots & \vdots \\ M_{a_{n1}}(\omega) & M_{a_{n2}}(\omega) & \dots & M_{a_{nn}}(\omega) \end{bmatrix} \tag{4}$$

$$\mathbf{R_r}(\omega) = \begin{bmatrix} R_{r_{11}}(\omega) & R_{r_{12}}(\omega) & \dots & R_{r_{1n}}(\omega) \\ R_{r_{21}}(\omega) & R_{r_{22}}(\omega) & \dots & R_{r_{2n}}(\omega) \\ \vdots & \vdots & \ddots & \vdots \\ R_{r_{n1}}(\omega) & R_{r_{n2}}(\omega) & \dots & R_{r_{nn}}(\omega) \end{bmatrix} \tag{5}$$

$$\mathbf{K_h} = \begin{bmatrix} K_{h_{11}} & 0 & \dots & 0 \\ 0 & K_{h_{22}} & \dots & 0 \\ \vdots & \vdots & \ddots & \vdots \\ 0 & 0 & \dots & K_{h_{nn}} \end{bmatrix} \tag{6}$$

The displacement vector and excitation force vector can be expressed as

$$\overrightarrow{\mathbf{Z}}(\omega) = \begin{bmatrix} \hat{z}_1(\omega) \\ \hat{z}_2(\omega) \\ \vdots \\ \hat{z}_n(\omega) \end{bmatrix} \tag{7}$$

$$\overrightarrow{\mathbf{F}_e}(\omega) = \begin{bmatrix} \hat{F}_{e_1}(\omega) \\ \hat{F}_{e_2}(\omega) \\ \vdots \\ \hat{F}_{e_n}(\omega) \end{bmatrix} \tag{8}$$

The hydrodynamic coefficients of the WEC array are numerically derived by an open-source boundary element method (BEM) solver, NEMOH. The hydrodynamic interactions between individual devices, including radiation and diffraction effects, are included in the calculation. The frequency range is specified as $[0.2\ rad/s, 3.1\ rad/s]$, containing 200 frequency components in total. It is acknowledged that the hydrodynamic modeling utilized in this work is based on linear potential flow theory. In this sense, the established model is inherently limited to small wave conditions where the nonlinearities in the system are not pronounced [17].

As described previously, the PTO system in each WEC is simplified to be a linear passive damper. Thus, the PTO force of each WEC is given as

$$\overrightarrow{\mathbf{F}}_{pto}(\omega) = -j\omega \mathbf{R_{pto}} \overrightarrow{\mathbf{Z}}(\omega) \tag{9}$$

As each WEC has an independent PTO system, there is no coupling effect between PTO systems of the WEC array. In this sense, the non-diagonal elements in $\mathbf{R_{pto}}$ are all defined to be zero, given as

$$\mathbf{R_{pto}} = \begin{bmatrix} R_{pto_{11}} & 0 & \dots & 0 \\ 0 & R_{pto_{22}} & \dots & 0 \\ \vdots & \vdots & \ddots & \vdots \\ 0 & 0 & \dots & R_{pto_{nn}} \end{bmatrix} \tag{10}$$

It is noted that the tuning of PTO damping is influential to the power performance of WEC arrays. A PTO damping tuning strategy was proposed in [18] for stand-alone WECs to maximize the power absorption, which is applied in the current work to determine the PTO damping value for each WEC in the array. Thus, the PTO damping of individual WEC in the array is given as

$$R_{pto_{ii}}(\omega) = \sqrt{B_{r_{ii}}(\omega)^2 + X_{ii}(\omega)^2} \tag{11}$$

where $R_{pto_{ii}}(\omega)$ is the tuned PTO damping for the i_{th} WEC at the specified wave frequency ω. The on-diagonal element in the intrinsic reactance X_{ii} is expressed as

$$X_{ii}(\omega) = \omega[M_{a_{ii}}(\omega) + M_{ii}(\omega)] - \frac{K_{h_{ii}}}{\omega} \tag{12}$$

where $M_{a_{ii}}$, M_{ii}, and $K_{h_{ii}}$ are the element located in the i_{th} row and the i_{th} column of the matrix $\mathbf{M_a}$, $\mathbf{M}$ and $\mathbf{K_h}$ respectively.

The optimal PTO damping, B_{pto}, is inherently frequency-dependent, indicating that this method was initially designed for application under regular wave conditions. To adapt it for irregular sea states, the energy period, T_e, is employed as an equivalent to the wave period in regular wave scenarios. Besides, the coupling effects between WECs are neglected in such a PTO tuning

strategy since only diagonal elements are involved in the calculation of the PTO damping. In addition, the derived PTO damping normally applies to the operational regions of WECs, in which nonlinear effects are negligible.

The PTO size of each WEC is represented by the PTO force constraint. To describe this effect, a nonlinear saturation function has to be implemented, which is illustrated in Figure 3. However, this represents a simplification, as the influence of PTO size on its dynamic behavior is neglected in this study. To comprehensively assess the impact of PTO sizing, it would be necessary to account for the variation of PTO losses and dynamics with PTO size. Nevertheless, given the scope and objectives of this work, this assumption is considered reasonable for providing a preliminary assessment of the effects of PTO sizing on the techno-economic performance of WEC arrays. The PTO force would be saturated once it reaches the defined PTO force limit. As the conventional frequency-domain modeling approach cannot incorporate nonlinearities, a computationally-efficient alternative, SD modeling, is adopted to address the PTO force saturation. In the SD model, the nonlinear terms are replaced in the equation of motion by linear equivalent coefficients via statistical linearization. The application of the SD modeling approach to WEC arrays has been investigated in a few of studies, marked by some pioneering work [19, 20] to recent advancement [21]. The SD models were developed and verified to evaluate the performance of WEC arrays with considering a variety of factors, such as wave climate, array configurations, and control strategies. As demonstrated in [22], the linear equivalent PTO damping of the PTO force saturation is given as

$$
\begin{aligned}
R_{eq,pto_{ii}} = {} & \frac{2R_{pto,ii}}{\sigma_{\dot{z}_i}^3\sqrt{2\pi}}\left[\frac{\sqrt{\pi}\sigma_{\dot{z}_i}^3\,\mathrm{erf}\left(\frac{\frac{F_{\mathrm{limit},i}}{R_{pto_{ii}}}}{\sqrt{2}\sigma_u}\right)}{\sqrt{2}}\right] \\
& - \frac{2R_{pto}}{\sigma_{\dot{z}_i}^3\sqrt{2\pi}}\left[\sigma_{\dot{z}_i}^2\left(\frac{F_{\mathrm{limit},i}}{R_{pto_{ii}}}\right)\exp\left(-\frac{\left(\frac{F_{\mathrm{limit},i}}{R_{pto_{ii}}}\right)^2}{2\sigma_{\dot{z}_i}^2}\right)\right] \\
& + \frac{2R_{pto}\left(\frac{F_{\mathrm{limit},i}}{R_{pto_{ii}}}\right)\sqrt{2\pi}}{\sigma_{\dot{z}_i}}\exp\left(-\frac{\left(\frac{F_{\mathrm{limit},i}}{R_{pto_{ii}}}\right)^2}{2\sigma_{\dot{z}_i}^2}\right)
\end{aligned}
\tag{13}
$$

where "erf" represents the error function; where $F_{\mathrm{limit},i}$ embodies the PTO force limit of the i_{th} WEC in the array; $\sigma_{\dot{z}_i}$ represents the standard deviation of the velocity of i_{th} WEC. The equivalent

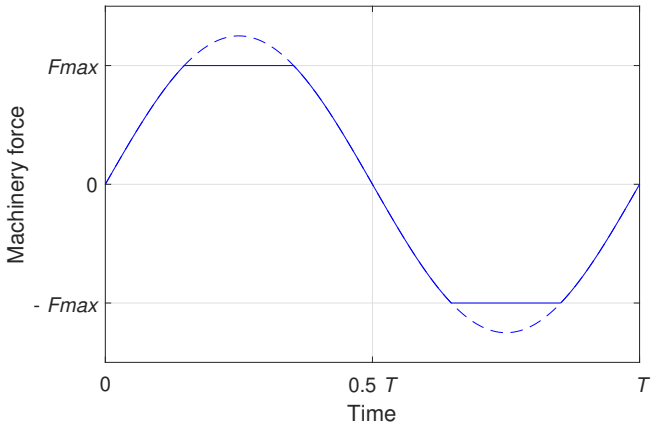

FIGURE 3: SCHEMATIC OF THE PTO MACHINERY FORCE SATURATION.

PTO damping matrix is written as

$$
\mathbf{R_{eq,pto}} = \begin{bmatrix} R_{eq,pto_{11}} & 0 & \dots & 0 \\ 0 & R_{eq,pto_{22}} & \dots & 0 \\ \vdots & \vdots & \ddots & \vdots \\ 0 & 0 & \dots & R_{eq,pto_{nn}} \end{bmatrix} \tag{14}
$$

As a consequence, the equation of motion in the SD model can be extended from (2) to

$$
\begin{aligned}
& -\omega^2\left(\mathbf{M}+\mathbf{M_a}(\omega)\right)\overrightarrow{\mathbf{Z}}(\omega) + j\omega\left(\mathbf{R_v}+\mathbf{R_r}(\omega)+\mathbf{R_{eq,pto}}\right)\overrightarrow{\mathbf{Z}}(\omega) \\
& +\mathbf{K_h}\overrightarrow{\mathbf{Z}}(\omega) = \overrightarrow{\mathbf{F}_e}(\omega)
\end{aligned}
\tag{15}
$$

To solve this equation of motion, an iterative scheme is needed and it is implemented referring to [13]. After solving the equation, given in (15), the dynamic responses of the WEC array is derived. The power absorption of i_{th} WEC at one specific sea state is calculated as

$$
P_i(ss) = \sum_{k=1}^{k=N}\omega_k^2\frac{1}{2}R_{eq,pto_{ii}}|\hat{z}_i(\omega_k)| \tag{16}
$$

where P_i is the absorbed power of i_{th} WEC in the array, k means the k_{th} frequency component, ss embodies the considered sea state, and $\hat{z}_i$ is the element located in the i_{th} row in the displacement vector of the WEC array $\overrightarrow{\mathbf{Z}}$. The total power production of the WEC array is then obtained by summing up the power

absorbed by all individual WECs as

$$P_{total}(ss) = \sum_{i=1}^{i=n} P_i \tag{17}$$

In the power calculation, the JONSWAP spectrum is applied to represent the irregular waves in the simulation of the WEC dynamics, and the peakedness factor is selected as 3.3. Each generated sea state consists of 200 harmonic wave components whose angular frequencies are evenly spaced from 0.2 rad/s to 3.1 rad/s.

3.2 Economic modeling

An economic model is developed to estimate the LCOE of the WEC array deployed at the European sea site near Yeu Island, located off the Vendée coast in western France. The scatter diagram for Yeu Island is illustrated in Fig. 4, where T_z and H_s denote the mean zero-crossing wave period and the significant wave height, respectively. Sea states with H_s exceeding 5 meters are excluded from the analysis, as these are considered beyond the operational limits of the WEC. The zero-crossing period T_z is converted into the peak period T_p by applying a factor of 1.287, consistent with the JONSWAP spectrum [23, 24].

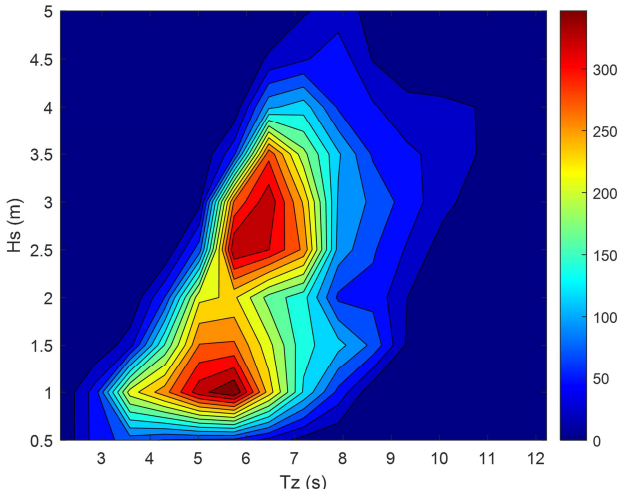

FIGURE 4: HOURS OF OCCURRENCE OF SEA STATES IN YEU ISLAND [25].

The CAPEX of WECs is composed by the mass related cost C_{Mass} and the power related cost C_{Power}, expressed as

$$\text{CAPEX} = C_{Mass} + C_{Power} \tag{18}$$

where C_{Mass} and C_{Power} can be calculated as

$$C_{Mass} = C_S + C_{F\&M} + C_I = (\frac{P_{F\&M}}{P_S} + \frac{P_I}{P_S} + 1)C_S \tag{19}$$

$$C_{Power} = C_{PTO} + C_C = (\frac{P_C}{P_P} + 1)C_{PTO} \tag{20}$$

where C_S, $C_{F\&M}$, and C_I represent the costs associated with the structure, foundation & mooring, and installation, respectively. C_{PTO} and C_C are the costs of the PTO and grid connection, while P_s, $P_{F\&M}$, P_I, P_P, and P_C are their respective percentages of the total CAPEX, as detailed in Table 2 [18].

Referring to the reports [26, 27], the marine stainless steel price, as of Q3 in 2024, was 3670 US dollars per metric tonne in the Europe market, and the hot-rolled band steel was around 750 US dollars per metric tonne. Given the fact that offshore structure manufacturing requires the combined use of multiple types of steel. The average steel price of the WEC structure is roughly estimated to be 1 Euro/kg, considering the currency exchange rate of 1.06. The PTO system is considered a direct drive generator, and all associated costs are attributed to it. The required active material depends on the generator's force limit and the force density. Based on [28], the maximum force density is taken to be 44 kN/m^2, typically varying from 30 to 60 kN/m^2 depending on the design. The active material cost is estimated at 14,600 Euros/m^2 [18, 28], with the total PTO cost being twice this value to account for manufacturing. In addition, the operational cost (OPEX) is assumed to be 8% of the CAPEX, with a discount rate of 8% and a 20-year lifespan, based on [29]. The LCOE of WECs is then calculated as:

$$\text{LCOE} = \frac{\text{CAPEX} + \sum_{t=1}^{Y} \frac{\text{OPEX}_t}{(1+r)^t}}{\sum_{t=1}^{Y} \frac{\text{AEP}_t}{(1+r)^t}} \tag{21}$$

where Y represents the total years of the lifespan, and t represents the evaluated year. The annual energy production (AEP) of the WEC at the sea site is calculated as

$$\text{AEP} = A \sum_{ss=1}^{ss=S} \varepsilon P_{total}(ss) T(ss) \tag{22}$$

where ε is the overall conversion efficiency from absorbed energy to AEP, set to 0.7 [30]; A is the WEC availability, taken as 0.9 to account for operation and maintenance [31]; T represents the total hours a given sea state occurs, shown in Fig. 4; ss is the sea state, and S is the total number of sea states considered.

TABLE 2: Percentages of CAPEX related components of WECs in total CAPEX [18].

CAPEX	Categories	Average Percentage
Mass-related capital cost	Structure	P_S =38.2%
	Foundation and mooring	$P_{F\&M}$=19.1%
	Installation	P_I =10.2%
Power-related capital cost	PTO component	P_P =24.2%
	Connection	P_C =8.3%

It should be noted that this is a preliminary economic model, and the parameter values vary across projects and are site-specific. For example, the operation availability and lifespan of WECs depend on factors such as wave resources, WEC designs, and PTO control strategies. In this paper, reference values are used to estimate the LCOE, aiming to provide a preliminary indication of how PTO sizing affects the economics of WEC arrays. Detailed LCOE studies for different WECs are presented in [1, 14, 18, 32].

3.3 PTO sizing optimization

An optimization problem is set up in this study to search the optimal PTO size for each individual WEC within the array. The objective of the optimization program is to minimize the LCOE of the WEC array, and the optimization variables are the PTO force limits of each WEC. This can be described as follows:

$$\begin{aligned} &\textit{minimize} \quad f = \mathrm{LCOE}(F_{\mathrm{limit},1}, F_{\mathrm{limit},2}, \cdots, F_{\mathrm{limit},n}) \\ &\textit{subject to} \left\{ F_{\mathrm{limit},n} \geq 0 \right\}. \end{aligned} \tag{23}$$

where $F_{\mathrm{limit},i}$ embodies the PTO force limit of the i_{th} WEC in the WEC array. In this sense, the objective function is related to n variables. However, considering the symmetry, it is only necessary to implement three independent variables. For instance, in the optimization of the WEC array layout 1, the WEC 1 and the WEC 2 share the same PTO force limit. It is noted that this symmetry doesn't hold when the directional waves are considered. The optimization is performed by the brute-force search. The searching area of the PTO force for each variable is defined to be $(12\ \mathrm{kN}, 100\ \mathrm{kN})$, and the searching step is set to be 2 kN.

4 Results and Discussion

4.1 Power performance of different WEC arrays

The total power absorption of different WEC array layouts is presented in Figure 5, in which the PTO force is unconstrained. For a better comparison, the power absorption of the WEC array layout 2 and layout 3 is depicted as the normalized values to that of the WEC array layout 1. It can be seen that the normalized values of the WEC array layout 2 and layout 3 are higher than 1 over a range of peak periods, which indicates that the WEC array layout 2 and layout 3 are associated with relatively higher power production. Besides, it is visible that the comparison of the power performance of WEC arrays is related to the peak periods. For instance, the WEC array layout 3 is more productive than layout 2 at the peak period of 6 s, while it turns to be less when the period is greater than 6 s.

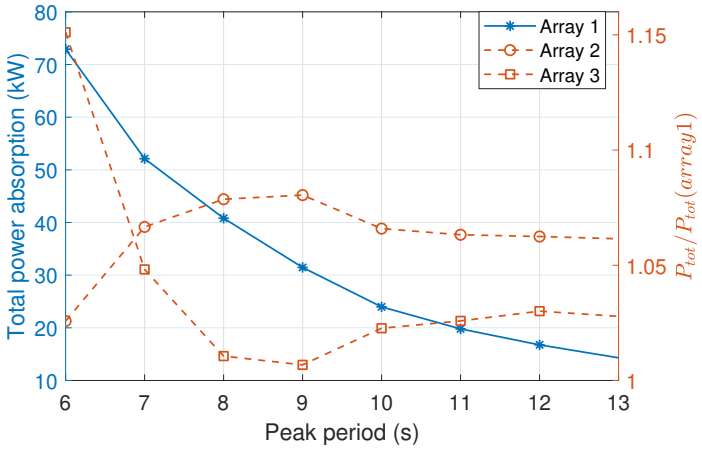

FIGURE 5: THE TOTAL POWER ABSORPTION OF THE WEC ARRAY LAYOUT 1, AND THE NORMALIZED POWER ABSORPTION OF THE ARRAY LAYOUT 2 AND LAYOUT 3 TO THAT OF THE LAYOUT 1 ($H_s = 2$ m) P_{TOT} REPRESENTS THE TOTAL POWER ABSORPTION OF THE SPECIFIED ARRAY LAYOUT. THE PTO SIZES FOR THE WECS IS UNCONSTRAINED.

To demonstrate the influence of the array interaction on individual WECs, the values of the modified q factor q_{mod} of the WECs are presented and compared for different WEC array configurations, as provided in Figure 6. Considering the symmetry

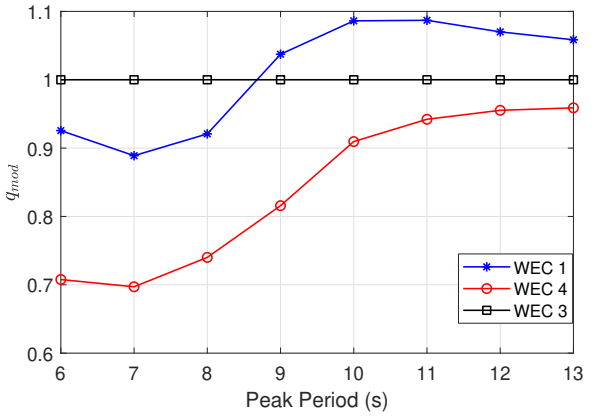

(a) WEC array layout 1

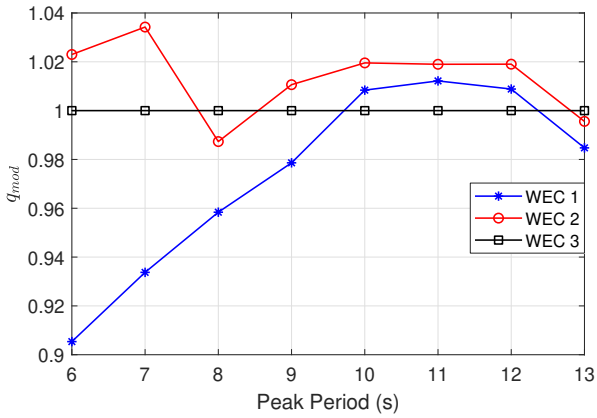

(b) WEC array layout 2

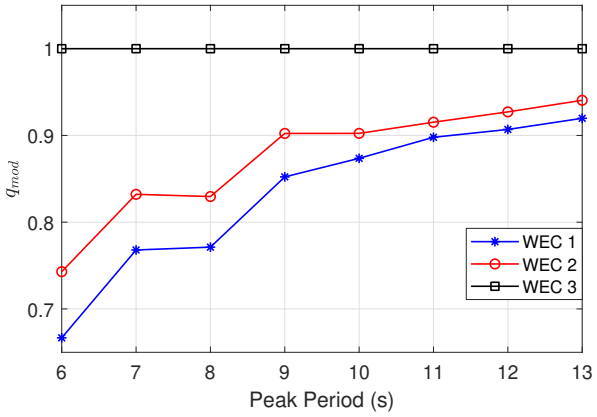

(c) WEC array layout 3

FIGURE 6: MODIFIED q FACTORS, q_{mod}, FOR DIFFERENT WEC ARRAY CONFIGURATIONS. WEC 3 IN EACH LAYOUT IS CONSIDERED AS THE REFERENCE IN THE CALCULATION OF THE MODIFIED Q FACTORS. THE PTO SIZES FOR THE WECS ARE UNCONSTRAINED. ($H_s = 2$ m)

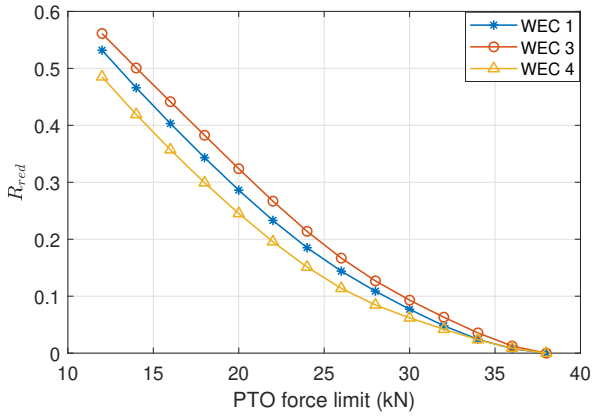

(a) WEC array layout 1

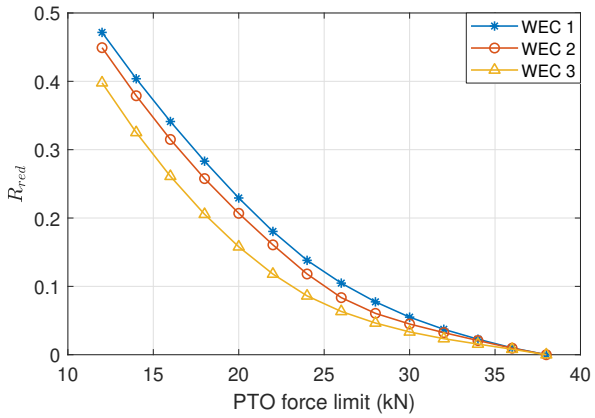

(b) WEC array layout 2

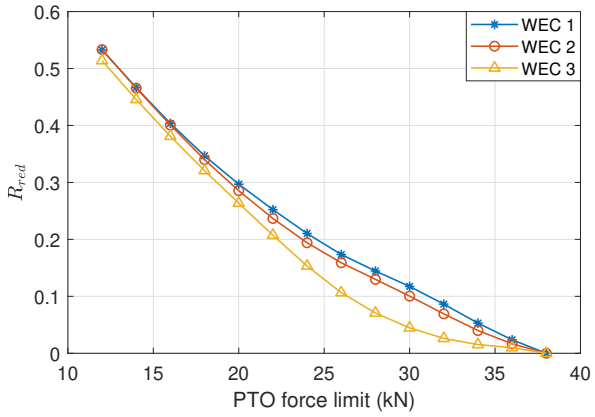

(c) WEC array layout 3

FIGURE 7: THE CALCULATED POWER REDUCTION RATIOS FOR DIFFERENT WEC ARRAYS. ONLY UPPER HALF OF EACH WEC ARRAY IS DEPICTED HERE GIVEN THE SYMMETRY. ($H_s = 2$ m; $T_p = 8$ s)

of the defined WEC array layouts in this work, only half of the

WECs above the x-axis are presented in the Figure. As the WEC 3 is located at the central line in every array layout, it is used as the normalization reference in the definition of the modified q factor, as formulated in (6). It can be deduced that the more different the modified q factors in the array layout are, the stronger the interaction of the WEC array. It is noticed that the WECs in the array layout 2 have more uniform power production, by comparing Figure 6(b) with Figure 6(a) and (c). For instance, the lowest and largest values of the modified q factor for the WEC array layout 2 are around 0.9 and 1.04. Comparatively, the calculated lowest values for the array layout 1 and layout 3 are approximately 0.7 and 0.65. This is thought to be reasonable, given the geometrical configurations of the arrays. Specifically, all five WECs are evenly spaced along a vertical line, which is expected to induce less hydrodynamic interaction compared with the other two considered WEC arrays. In addition, it is noted that the modified q factor presents a clear correlation with the peak periods. For example, in Figure 6(c), the modified q factor of the WEC 1 increases from 0.65 to over 0.9. This results from the fact that the hydrodynamic interactions in an array are realized by the radiation and diffraction of the WECs. The variation of the wave periods and then the oscillation period of the WECs would result in changes in the wavelengths of both radiated waves and diffracted waves. However, the relative distances of the WECs in a WEC array are fixed. Consequently, the changed wave lengths inevitably lead to different characteristics of the hydrodynamic interactions.

4.2 The effect of the PTO size on the power production

The PTO size is associated with the maximum force the PTO system could handle. Hence, the PTO size is expected to make a difference in the dynamics and then the power absorption of the WEC system. Given the interaction between WECs, the effect of PTO sizing on the power absorption of the individual WEC is related to its position in the array. To better demonstrate the effect, a parameter "power reduction ratio" is introduced for the individual WEC, named "R_{red}", as

$$R_{red} = \frac{P_i(unconstrained) - P_i(F_{limit,i})}{P_i(unconstrained)} \tag{24}$$

where $P_i(unconstrained)$ and $P_i(F_{limit,i})$ mean the power absorption of i_{th} WEC without the PTO force constraint and that with the PTO force limit F_{limit} applied to all WECs in the array. R_{red} is the power reduction ratio, which indicates how much the imposed PTO force limit reduces the power absorption.

Figure 7 illustrates the power reduction ratio of WECs in different array configurations. It is easy to observe the variations of the power reduction ratios of WECs in all the array layouts. For instance, in Figure 7(a), the power reduction ratio for the WEC 4 is 0.25 while it is around 0.33 when the PTO force limit is 20 kN. It corresponds to a difference of 24 %. This implies the necessity of implementing the PTO sizing for individual devices in a WEC array. In addition, it can be found by comparing the three subfigures that the power reduction ratios have a strong relation with the array configuration. In Figure 7(a), the WEC 3, known as the centrally located one, has a higher power reduction ratio than other individual WECs. However, in Figure 7(b), the WEC 3 has the lowest power reduction ratios. In addition, when the PTO force limit is decreased below 12 kN, the power reduction ratios of WECs in array layout 3 are more comparable than those in the WEC array layout 1 and 2. The relative deviations of the power reduction ratios of WECs in the WEC array 3 are no more than 10 %. It is inferred that the PTO sizing effect on individual WECs would differ depending on the specific array configurations.

4.3 PTO sizing optimization in WEC arrays

The obtained optimal PTO sizes of individual WECs in different array layouts are presented in Table 3, and the corresponding values of the LCOE are given in Table 4. It can be noticed in Table 3 that the individual WECs are associated with the varied optimal PTO sizes, even in the same WEC array configuration. For example, in the WEC array layout 3, the WEC 1 and WEC 5 have an optimized PTO size of 38 kN, while the optimized PTO size for the WEC 2,3 and 4 is 44 kN. This marks a difference of over 10 %. Furthermore, It can be seen that the array configuration has a clear influence on the PTO size optimization. For instance, the centrally-located WEC, WEC 3, has the optimal PTO force limit of 40 kN, 36 kN and 44 kN for the layouts 1, 2 and 3 respectively. Therefore, the PTO sizing is highly array configuration-specific and it is suggested to conduct the PTO sizing together with the array optimization for the sake of a better techno-economic performance.

The values of the LCOE and the AEP of WEC arrays with the optimized PTO sizes are provided in Table 4 and 5. For comparison, the LCOE and the AEP are calculated for WECs without implementing any PTO size optimization, named "Non-Optimized" in the tables. The PTO force limits for all the WECs are defined to be 65 kN, by which the WEC array layout 1 could operate at full capacity at the most powerful sea state occurring at the sea site [18]. The sea state is characterized as $H_s = 4\ m$ and $T_z = 10\ s$. Table 5 suggests that the optimized PTO sizes lead to the reduction of the AEP in all the considered array configurations, in which the reduction could reach 9 %. However, an improved techno-economic performance of the WEC arrays can be achieved by implementing the PTO sizing for individual WECs. As depicted in Table 4, the PTO size optimization for individual WECs in arrays could reduce the LCOE by around 10 % to 14 %, depending on the array configurations.

TABLE 3: THE OPTIMAL PTO FORCE LIMIT OF EACH WEC IN THE THREE ARRAY CONFIGURATIONS

	Layout 1	**Layout 2**	**Layout 3**
WEC 1	42 kN	36 kN	38 kN
WEC 2	42 kN	38 kN	44 kN
WEC 3	40 kN	36 kN	44 kN
WEC 4	38 kN	38 kN	44 kN
WEC 5	38 kN	36 kN	38 kN

TABLE 4: THE VALUES OF THE LCOE WITH AND WITHOUT THE PTO SIZE OPTIMIZATION

	Optimized (Euros/kWh)	**Non-Optimized** (Euros/kWh)	**Deviation**
Layout 1	0.3185	0.3618	12 %
Layout 2	0.3020	0.3514	14 %
Layout 3	0.3150	0.3519	10 %

TABLE 5: THE VALUES OF THE AEP WITH AND WITHOUT THE PTO SIZE OPTIMIZATION

	Optimized (MWh)	**Non-Optimized** (MWh)	**Deviation**
Layout 1	271	295	8 %
Layout 2	277	304	9 %
Layout 3	278	303	8 %

5 Conclusion

In this paper, a study is carried out to reveal the interplay between the power performance, the PTO sizing and the techno-economic performance of WECs on an array scale. Three different WEC array configurations are implemented, and all the considered arrays contain five spherical point absorbers. The SD modeling approach is utilized to estimate the dynamics and the power performance of the WEC arrays. The PTO size is represented by the maximal PTO force allowed by the system. In the SD modeling, the statistical linearization method is applied to cope with the nonlinearity introduced by the effect of the PTO force limit on the dynamics. Additionally, a preliminary economic model is also built to calculate the cost of the WEC array with the varied PTO sizes. Furthermore, an optimization program of PTO sizes for individual WECs is performed for the three arrays, in which a realistic sea site is taken into account. The conclusions are drawn as follows.

First, the imposed PTO force limit would penalize the power absorption of all WECs in an array. Generally, The smaller the PTO force limit, the more reduction of the power absorption occurs. However, the individual WECs within an array are associated with different reactions to the effect of the PTO force limit. The deviations of power reduction ratios of WECs within one array could even reach 24 % in particular sea states.

Secondly, the array configuration could make a difference in the effect of PTO sizing on the power performance of individual WECs. When the PTO force limit is restrained to 20 kN, the difference in the power reduction ratios of the WECs could range from 10 % to 24 % in the three considered configurations. In this sense, it implies the importance of incorporating the PTO sizing into the optimization of the WEC array configurations.

Thirdly, the optimized PTO force limits of individual WECs vary even in the same array. Particularly, in the WEC array layout 3, the largest value of the optimized PTO force limits arrives at 44 kN while the smallest is 38 kN. This indicates the significance of implementing the PTO sizing for individual WECs in an array. Furthermore, the PTO size optimization doesn't necessarily contribute to the largest AEP, but it could reduce the LCOE by 10 % to 14 % compared to WEC arrays without optimizing the PTO sizes.

REFERENCES

[1] De Andres, A., Medina-Lopez, E., Crooks, D., Roberts, O., and Jeffrey, H., 2017. "On the reversed LCOE calculation: Design constraints for wave energy commercialization". *International Journal of Marine Energy,* ***18***, pp. 88–108.

[2] Sharp, C., and DuPont, B., 2015. "Wave energy converter array optimization: A review of current work and preliminary results of a genetic algorithm approach introducing cost factors". In International Design Engineering Technical Conferences and Computers and Information in Engineering Conference, Vol. 57076, American Society of Mechanical Engineers, p. V02AT03A025.

[3] Liu, Z., Wang, Y., and Hua, X., 2021. "Proposal of a novel analytical wake model and array optimization of oscillating wave surge converter using differential evolution algorithm". *Ocean Engineering,* ***219***, p. 108380.

[4] Penalba, M., Giorgi, G., and Ringwood, J. V., 2017. "Mathematical modelling of wave energy converters: A review of nonlinear approaches". *Renewable and Sustainable Energy Reviews,* ***78***, pp. 1188–1207.

[5] Göteman, M., Engström, J., Eriksson, M., and Isberg, J., 2015. "Optimizing wave energy parks with over 1000 interacting point-absorbers using an approximate analytical

method". *International Journal of Marine Energy,* ***10***, pp. 113–126.

[6] Lyu, J., Abdelkhalik, O., and Gauchia, L., 2019. "Optimization of dimensions and layout of an array of wave energy converters". *Ocean Engineering,* ***192***, p. 106543.

[7] Tan, J., Polinder, H., Wellens, P., and Miedema, S., 2020. "A feasibility study on downsizing of power take off system of wave energy converters". In *Developments in Renewable Energies Offshore*. CRC Press, pp. 140–148.

[8] Tan, J., Wang, X., Jarquin Laguna, A., Polinder, H., and Miedema, S., 2021. "The influence of linear permanent magnet generator sizing on the techno-economic performance of a wave energy converter". In 2021 13th International Symposium on Linear Drives for Industry Applications (LDIA), pp. 1–6.

[9] Tan, J., Polinder, H., Laguna, A. J., and Miedema, S., 2023. "A wave-to-wire analysis of the adjustable draft point absorber wave energy converter coupled with a linear permanent-magnet generator". *Ocean Engineering,* ***276***, p. 114195.

[10] Tan, J., Polinder, H., Laguna, A. J., and Miedema, S., 2022. "A numerical study on the performance of the point absorber wave energy converter integrated with an adjustable draft system". *Ocean Engineering,* ***254***, p. 111347.

[11] Tan, J., and Laguna, A. J., 2023. "Spectral-domain modelling of wave energy converters as an efficient tool for adjustment of pto model parameters". In Proceedings of the European Wave and Tidal Energy Conference, Vol. 15.

[12] Tan, J., Tao, W., Laguna, A. J., Polinder, H., Xing, Y., and Miedema, S., 2023. "A spectral-domain wave-to-wire model of wave energy converters". *Applied Ocean Research,* ***138***, p. 103650.

[13] Tan, J., Polinder, H., Laguna, A. J., and Miedema, S., 2022. "The application of the spectral domain modeling to the power take-off sizing of heaving wave energy converters". *Applied Ocean Research,* ***122***, p. 103110.

[14] Tan, J., Wang, X., Polinder, H., Laguna, A. J., and Miedema, S. A., 2022. "Downsizing the linear pm generator in wave energy conversion for improved economic feasibility". *Journal of Marine Science and Engineering,* ***10***(9), p. 1316.

[15] Tan, J., Jarquin Laguna, A., Polinder, H., and Miedema, S., 2022. "The application of the spectral domain modeling to the techno-economic analysis of the adjustable draft point absorbers". In International Conference on Offshore Mechanics and Arctic Engineering, Vol. 85932, American Society of Mechanical Engineers, p. V008T09A067.

[16] Folley, M., Babarit, A., Child, B., Forehand, D., O'Boyle, L., Silverthorne, K., Spinneken, J., Stratigaki, V., and Troch, P., 2012. "A review of numerical modelling of wave energy converter arrays". In International Conference on Offshore Mechanics and Arctic Engineering, Vol. 44946, American Society of Mechanical Engineers, pp. 535–545.

[17] , 2016. *Numerical Modelling of Wave Energy Converters*.

[18] Tan, J., Polinder, H., Laguna, A. J., Wellens, P., and Miedema, S. A., 2021. "The influence of sizing of wave energy converters on the techno-economic performance". *Journal of Marine Science and Engineering,* ***9***(1), p. 52.

[19] Cruz, J., Sykes, R., Siddorn, P., and Taylor, R. E., 2009. "Wave farm design: preliminary studies on the influences of wave climate, array layout and farm control".

[20] Folley, M., and Whittaker, T., 2013. "Preliminary cross-validation of wave energy converter array interactions". In International Conference on Offshore Mechanics and Arctic Engineering, Vol. 55423, American Society of Mechanical Engineers, p. V008T09A055.

[21] Ermakov, A., Ali, Z. A., Mahmoodi, K., Mason, O., and Ringwood, J. V., 2024. "A frequency domain-based control methodology for performance assessment and optimisation of heterogeneous arrays of wave energy converters". In 2024 IEEE Conference on Control Technology and Applications (CCTA), IEEE, pp. 584–589.

[22] Tan, J., Polinder, H., Laguna, A. J., and Miedema, S., 2022. "The application of the spectral domain modeling to the power take-off sizing of heaving wave energy converters". *Applied Ocean Research,* ***122***, p. 103110.

[23] Myrhaug, D., and Kjeldsen, S. P., 1987. "Prediction of occurrences of steep and high waves in deep water". *Journal of waterway, port, coastal, and ocean engineering,* ***113***(2), pp. 122–138.

[24] Journée, J. M. J., Massie, W. W., and Huijsmans, R. H. M., 2015. *Offshore hydrodynamics*.

[25] Babarit, A., Hals, J., Muliawan, M. J., Kurniawan, A., Moan, T., and Krokstad, J., 2012. "Numerical benchmarking study of a selection of wave energy converters". *Renewable Energy,* ***41***, pp. 44–63.

[26] IMARC Group, 2024. Stainless steel pricing report. Accessed: 2024-12-19.

[27] Steel, S., 2024. Price for ah36 steel plate for shipbuilding. Accessed: 2024-12-19.

[28] Polinder, H., 2013. *Principles of electrical design of permanent magnet generators for direct drive renewable energy systems*. Woodhead Publishing Limited.

[29] De Andres, A., Maillet, J., Todalshaug, J. H., Möller, P., Bould, D., and Jeffrey, H., 2016. "Techno-economic related metrics for a wave energy converters feasibility assessment". *Sustainability (Switzerland),* ***8***(11).

[30] Chozas, J., Kofoed, J., and Helstrup, N., 2014. "The COE Calculation Tool for Wave Energy Converters (Version 1 . 6 , April 2014)".

[31] Kramer, M. M., Marquis, L., and Frigaard, P., 2011. "Performance Evaluation of the Wavestar Prototype". *Proceedings of the 9th European Wave and Tidal Conference*, pp. 5–9.

[32] O'Connor, M., Lewis, T., and Dalton, G., 2013. "Techno-economic performance of the Pelamis P1 and Wavestar at different ratings and various locations in Europe". *Renewable Energy,* ***50***, pp. 889–900.